AGU PUBLICATIONS

JGR

Journal of Geophysical Research: Atmospheres

RESEARCH ARTICLE
10.1002/2015JD023382

Key Points:
- Absorption enhancement through lensing not relevant for black carbon in Toronto
- Brown carbon responsible for over 50% of direct absorption at 405 nm at times
- Thermal denuding at 250°C ineffective for removal of wildfire NR-PMBC

Supporting Information:
- Supporting Information S1
- Figure S1
- Figure S2
- Figure S3
- Figure S4

Correspondence to:
R. M. Healy,
robert.healy@utoronto.ca

Citation:
Healy, R. M., et al. (2015), Light-absorbing properties of ambient black carbon and brown carbon from fossil fuel and biomass burning sources, *J. Geophys. Res. Atmos.*, *120*, 6619–6633, doi:10.1002/2015JD023382.

Received 13 MAR 2015
Accepted 16 JUN 2015
Accepted article online 18 JUN 2015
Published online 14 JUL 2015

Light-absorbing properties of ambient black carbon and brown carbon from fossil fuel and biomass burning sources

R. M. Healy[1,2], J. M. Wang[1], C.-H. Jeong[1], A. K. Y. Lee[3], M. D. Willis[3], E. Jaroudi[1], N. Zimmerman[1], N. Hilker[1], M. Murphy[1], S. Eckhardt[4], A. Stohl[4], J. P. D. Abbatt[3], J. C. Wenger[2], and G. J. Evans[1]

[1]Southern Ontario Centre for Atmospheric Aerosol Research, University of Toronto, Toronto, Ontario, Canada, [2]Department of Chemistry and Environmental Research Institute, University College Cork, Cork, Ireland, [3]Department of Chemistry, University of Toronto, Toronto, Ontario, Canada, [4]Norwegian Institute for Air Research, Kjeller, Norway

Abstract The optical properties of ambient black carbon-containing particles and the composition of their associated coatings were investigated at a downtown site in Toronto, Canada, for 2 weeks in June 2013. The objective was to assess the relationship between black carbon (BC) coating composition/thickness and absorption. The site was influenced by emissions from local vehicular traffic, wildfires in Quebec, and transboundary fossil fuel combustion emissions in the United States. Mass concentrations of BC and associated nonrefractory coatings were measured using a soot particle–aerosol mass spectrometer (SP-AMS), while aerosol absorption and scattering were measured using a photoacoustic soot spectrometer (PASS). Absorption enhancement was investigated both by comparing ambient and thermally denuded PASS absorption data and by relating absorption data to BC mass concentrations measured using the SP-AMS. Minimal absorption enhancement attributable to lensing at 781 nm was observed for BC using both approaches. However, brown carbon was detected when the site was influenced by wildfire emissions originating in Quebec. BC coating to core mass ratios were highest during this period (~7), and while direct absorption by brown carbon resulted in an absorption enhancement at 405 nm (>2.0), no enhancement attributable to lensing at 781 nm was observed. The efficiency of BC coating removal in the denuder decreased substantially when wildfire-related organics were present and may represent an obstacle for future similar studies. These findings indicate that BC absorption enhancement due to lensing is minimal for downtown Toronto, and potentially other urban locations, even when impacted by long-range transport events.

1. Introduction

Black carbon-containing particles, produced through the incomplete combustion of fossil fuels and biomass, directly absorb incoming solar radiation across all visible wavelengths and exert a positive atmospheric radiative forcing [*Horvath*, 1993; *Jacobson*, 2000; *Bond et al.*, 2013]. While the role of atmospheric particles in the formation of water and ice clouds introduces the highest uncertainty associated with current global radiative forcing estimates, the absorption efficiency of internally mixed black carbon (BC) particles is also poorly constrained [*Intergovernmental Panel on Climate Change*, 2013]. BC particles often contain internally mixed organics upon emission, with the ratio of BC to organics dependent on the fuel type and efficiency of combustion [*Bond et al.*, 2013; *Martin et al.*, 2013]. BC particles may also accumulate significant secondary inorganic and organic coatings through atmospheric processing, affecting their cloud condensation nuclei activity, hygroscopicity, atmospheric lifetime, and potentially their mass absorption cross section (MAC) [*Jacobson*, 2001; *Riemer et al.*, 2004; *Bond et al.*, 2006; *Stier et al.*, 2006; *Cappa et al.*, 2012; *Liu et al.*, 2013].

In laboratory studies, significant absorption enhancement attributed to lensing of light has been observed for absorbing particles when they are coated with organic or inorganic species, including water [*Schnaiter et al.*, 2005; *Khalizov et al.*, 2009; *Lack et al.*, 2009; *Cappa et al.*, 2012]. Absorption enhancement (E_{abs}) in the wavelength range of 450–700 nm for laboratory-generated coated BC has been demonstrated to agree with Mie theory predictions for simple core-shell structures reasonably well [*Schnaiter et al.*, 2005; *Cross et al.*, 2009; *Cappa et al.*, 2012]. However, the magnitude of the lensing absorption enhancement is predicted to be reduced if the coating material itself also absorbs light effectively, for example, if brown carbon (BrC) coatings associated with biomass combustion are present [*Lack and Cappa*, 2010; *Lack et al.*, 2012;

Mohr et al., 2013; *Nakayama et al*., 2014]. Fresh diesel exhaust soot particles have been determined to exhibit no detectable E_{abs} (781 nm) through lensing by internally mixed organics [*Guo et al*., 2014]. On the other hand, absorption enhancements have been observed for laboratory measurements of fresh biomass burning BC, with the magnitude being strongly dependent on the coating to core mass ratio, with E_{abs} (781 nm) values ranging from 1.1 to 2.5 for coating to core ratios between 4 and 20 [*McMeeking et al*., 2014].

Single-particle measurements have also been used to predict absorption enhancement for internally mixed BC, but in the absence of detailed morphology data [*Schwarz et al*., 2008] (1064 nm), [*Moffet and Prather*, 2009] (532 nm). Morphology can influence predicted E_{abs} significantly, but Mie theory "core-shell" models are often simplified by assuming a concentric spherical structure. Upon emission, BC particles tend to exhibit a fractal structure composed of smaller spherules [*Adachi et al*., 2010] which may collapse to a more closely packed shape when the particles accumulate enough coating material [*Weingartner et al*., 1995; *Fuller et al*., 1999; *Khalizov et al*., 2009; *Chan et al*., 2011; *Martin et al*., 2013; *Schnitzler et al*., 2014], This restructuring can potentially impact BC core MAC values [*Liu et al*., 2008]. Furthermore, BC inclusions, regardless of shape, will not necessarily lie in the center of a mixed particle [*Fuller et al*., 1999; *Adachi et al*., 2010; *Sedlacek et al*., 2012; *Adachi and Buseck*, 2013; *China et al*., 2013]. These morphological phenomena reduce the appropriateness of Mie theory core-shell predictions of E_{abs} for internally mixed BC [*Liu et al*., 2015], and thus measurements of E_{abs} in a variety of ambient environments are necessary to determine appropriate values for modeling purposes.

Cappa et al. [2012] determined that aged coated BC particles originating from urban centers, detected during two field campaigns in California, exhibited minimal absorption enhancement (532 nm) due to lensing by internally mixed nonrefractory material, despite significant photochemical aging. Absorption measurements were performed using photoacoustic spectroscopy. E_{abs} at 532 nm attributed to lensing was determined to be only 1.06 on average, approximately an order of magnitude lower than both the enhancement predicted by Mie core-shell theory and the enhancement observed for analogous laboratory-generated BC coated with liquid organics (dioctyl sebacate). Low-absorption enhancement (1.07–1.10, 532 and 781 nm) due to lensing has also been determined using the same technique for BC detected at urban sites in China and Japan [*Lan et al*., 2013; *Nakayama et al*., 2014]. However, E_{abs} values up to 1.7 (532 nm), and significant direct absorption by coemitted primary organic aerosol (MAC ~0.8 $m^2 g^{-1}$ at 404 nm), have been observed for BC in a wildfire plume [*Lack et al*., 2012]. *Lack et al*. [2012] ascertained that direct absorption by both BC and primary BrC, optical lensing, and the extent of internal mixing were all relevant factors contributing to total aerosol absorption in that case. Both the absence and presence of absorption enhancement through lensing have been demonstrated for BC in rural Ontario, but in separate field studies using different instruments, specifically a particle soot absorption photometer (567 nm) and photoacoustic soot spectrometer (PASS) (781 nm), respectively [*Chan et al*., 2010, 2011]. Thus, a range of E_{abs} values have been reported for BC from different sources and of varying photochemical age both in the laboratory and field. The use of different measurement techniques also complicates direct comparisons.

While aerosol in Toronto is predominantly associated with regional-scale traffic emissions, long-range transport of natural wildfire and anthropogenic emissions also periodically impacts local air quality significantly [*Jeong et al*., 2011, 2013]. Optical properties of ambient BC and thermally denuded BC have been investigated in Toronto previously using photoacoustic and thermal-optical elemental carbon data [*Knox et al*., 2009]. In that case, chemical mixing state and coating to core mass ratios could not be measured for BC directly; however, the data set was separated into periods influenced predominantly by fresh, semiaged, and aged aerosols using particle number-size distribution data, meteorological data, and bulk aerosol composition. BC E_{abs} at 760 nm was determined to be 1.2, 1.4, and ~1 for periods dominated by fresh, "semiaged," and aged aerosols, respectively. *Knox et al*. [2009] proposed that coatings on fresh and semiaged aerosols may have efficiently evaporated in the denuder, while more aged coatings were less volatile and thus were not removed.

In this study, light-absorbing properties of ambient aerosol in downtown Toronto were investigated over a 2 week period to assess whether internally mixed coating material, quantified using a soot particle–aerosol mass spectrometer, contributed to any detectable absorption enhancement effect for BC. Absorption enhancement at 405 and 781 nm, determined for periods influenced by local emissions, transported wildfire emissions originating in Quebec, and transboundary anthropogenic emissions in the northern United States are discussed.

2. Method

Measurements were performed from 12 to 25 June 2013 at the Southern Ontario Centre for Atmospheric Aerosol Research Facility, located in downtown Toronto, Canada (43.66°N, 79.40°W). The facility is located at ground level, adjacent to a road with traffic volumes ranging from 16,000 to 25,000 vehicles per day [*Sabaliauskas et al*., 2014]. Ambient air was sampled at 170 L min^{-1} through a 10 cm (inner diameter) stainless steel tube. The tube was fitted with a 2.5 μm cutoff inlet, located 15 m from the roadside at a height of 3 m (above ground level). All instruments used to measure the optical and chemical properties of BC particles were connected to this common sampling line.

A photoacoustic soot spectrometer (PASS-3, Droplet Measurement Techniques, Boulder, CO) was used to measure aerosol absorption (b_{abs}) and scattering (b_{sca}) coefficients (Mm^{-1}) at 405 and 781 nm. A 532 nm laser is not installed in this particular unit. The PASS-3 determines aerosol absorption (Mm^{-1}) in a cavity which acts as an acoustic resonator [*Arnott et al*., 1999]. The absorption of incoming radiation heats the particles, which in turn heat the surrounding air in the cavity. The aerosol-laden air thus expands, resulting in a pressure disturbance. By modulating the laser power at the resonance frequency of the cavity, the pressure disturbance is amplified and the resulting acoustic wave is measured using a microphone. Light scattering at both wavelengths is concurrently measured using reciprocal nephelometry [*Moosmüller et al*., 2009; *Flowers et al*., 2010; *Chan et al*., 2011].

A soot particle–aerosol mass spectrometer [*Onasch et al*., 2012] (SP-AMS, Aerodyne Research Inc., Billerica, MA) was used to quantitatively measure refractory black carbon (rBC) and nonrefractory BC coatings, specifically organics, ammonium, nitrate, and sulfate. For consistency with previous work, the BC coating material measured using the SP-AMS will be referred to here as NR-PM_{BC} (nonrefractory particulate matter internally mixed with BC) [*Cappa et al*., 2012; *McMeeking et al*., 2014]. Briefly, the SP-AMS is a high-resolution time-of-flight mass spectrometer fitted with a diode-pumped neodymium: yttrium/aluminum/garnet (Nd:YAG) 1064 nm laser vaporizer, which exclusively vaporizes those particles that absorb near-infrared radiation efficiently (such as metals and rBC). As the rBC particles are heated to ~4000 K and vaporized, any internally mixed coating material will also evaporate. The resulting gas phase species are ionized through electron impact (70 eV) and detected using a high-resolution mass spectrometer. The SP-AMS was operated with the tungsten thermal vaporizer removed to minimize any potential interference from externally mixed particles that do not contain rBC [*Willis et al*., 2014]. The instrument was operated alternately in three modes for the measurement of rBC particle ensembles (MS mode), size-resolved rBC particles ensembles (pToF), and single rBC particles (LSSP mode) [*Lee et al*., 2015]. Without the tungsten vaporizer, direct calibrations of the ionization efficiency for NH_4NO_3 (IE_{NO3}) were not possible. Thus, size-selected (300 nm) Regal Black (Regal 400R Pigment, Cabot Corp.) particles were used to determine the mass-based ionization efficiency of rBC (mIE_{BC}) [*Onasch et al*., 2012; *Willis et al*., 2014]. The relative ionization efficiency for BC (RIE_{BC}, defined as the ratio of the mass specific ionization efficiencies of rBC and NO_3, mIE_{BC}/mIE_{NO3}) was 0.2, as experimentally determined before removal of the tungsten vaporizer. Assuming that RIE_{BC} is the same with and without the tungsten vaporizer present, the IE_{NO3} could be calculated based on known values of mIE_{BC} and RIE_{BC}. The average mIE_{BC} was 189 ± 20 ions pg^{-1}. The calculated IE_{NO3} was then used with recommended relative ionization efficiencies to quantify NR-PM_{BC} species [*Jimenez et al*., 2003]. We have assumed here that the entire CO_2^+ and CO^+ signals are attributable to organics, but it should be noted that oxygenated moieties on rBC itself could also contribute [*Corbin et al*., 2014]. It is also possible that the assumption inherent in the organic fragmentation table of $CO_2^+ = CO^+$ is not accurate from CO_x^+ signals arising from rBC. Therefore, it is possible that we underestimate the CO^+/C_3^+ ratio for rBC, and the required experiments in a nitrogen-free atmosphere have not been carried out with our SP-AMS to determine an appropriate CO^+/C_3^+ ratio for ambient black carbon or a suitable surrogate. Given these limitations, we assume that $CO_2^+ = CO^+$ with the possibility that we are underestimating CO_x^+ mass. Collection efficiency for rBC particles, related to the overlap of the particle beam and the IR laser vaporizer, was determined on-site using beam width probe measurements described in *Willis et al*. [2014]. Ambient rBC-containing particles at this site had an average beam width $\sigma = 0.46 \pm 0.03$ mm, which is close to, but wider than that of 300 nm Regal Black particles ($\sigma = 0.40 \pm 0.08$) [*Willis et al*., 2014]. Therefore, a collection efficiency of 0.6 was applied to quantify rBC and NR-PM_{BC}. It is important to note that a time-varying CE would result in different rBC mass concentrations and MAC values. A higher CE of 1 was explored for

those periods when the site was influenced by nonlocal emissions but was found to reduce the linearity between PASS b_{abs} (781 nm) and rBC mass concentration.

An aerosol time-of-flight mass spectrometer (ATOFMS 3800, TSI Inc., Shoreview, MN) [*Gard et al*., 1997], fitted with an aerodynamic focusing lens (AFL 100) [*Su et al*., 2004], was used to investigate single-particle composition and mixing state in the size range of 200–3000 nm (d_{va}). Particles are pumped through a critical orifice to the aerodynamic lens where they are focused into a vertical beam before transmission to the sizing region. Particle velocity between two sizing lasers (532 nm) is used to determine d_{va}, calibrated using polystyrene latex spheres. A timing circuit is used to estimate the arrival time of each particle in the mass spectrometry region of the instrument where a Nd:YAG laser (266 nm) is triggered for desorption/ionization. Finally, a dual-polarity mass spectrum is collected for each particle successfully ionized using two time-of-flight mass spectrometers. Mass spectral data were imported using the ENCHILADA open source software package [*Gross et al*., 2010] and clustered using the *K*-means algorithm [*Rebotier and Prather*, 2007; *Healy et al*., 2013]. A *K* value of 60 was selected because larger *K* values did not appreciably reduce the average Euclidean distance of each particle to its assigned cluster centroid. The 60 clusters were manually merged to produce final "classes" representing particle types with differing primary and/or secondary chemical composition. Only those particles identified as potassium-rich, featuring positive ion mass spectra with *m/z* 39 as the highest-intensity peak, are discussed here.

A thermodenuder (Dekati Inc.), operated at 250°C with a flow rate of 6 L min^{-1}, was used to remove NR-PM_{BC} coatings associated with rBC. The residence time for particles in the heated section of the thermodenuder was 1.9 s. The PASS-3 instrument switched between sampling ambient aerosol and denuded aerosol every 10 min using an automated sampling valve, and zero measurements were taken after each valve switch. Thus, absorption enhancement (E_{abs}) at 405 and 781 nm was calculated by direct comparison of denuded and ambient data collected within the same hour, as shown in equation (1).

$$E_{abs} = \frac{b_{abs,\ ambient}}{b_{abs,\ denuded}} \tag{1}$$

In this case, $b_{abs,denuded}$ data must be corrected for rBC mass-based transmission efficiency, which was determined experimentally to be 72% at 250°C and 6 L min^{-1} using hourly resolution ambient and denuded data from the SP-AMS ($N = 93$). The experimental transmission efficiency is in good agreement with the theoretical transmission efficiency of the denuder for particles <70 nm in diameter, and for particles 70–500 nm in diameter, at the flow rate and temperature used here (73 and 75%, respectively). Calculating E_{abs} using the PASS-3 data exclusively is based on the assumption that the BC ensemble mass concentration and optical properties do not change within a 1 h period. However, because the sampling site is located next to a road, short-duration vehicle exhaust plumes are often observed. Vehicle plumes were removed using a recently developed algorithm based on particle number concentration temporal data measured at 1 Hz resolution using a fast mobility particle sizer (TSI Inc., Shoreview, MN) [*Wang et al*., 2015], providing a data set that is more representative of the urban background. Accounting for vehicle plumes removed 16% of the 0.5 Hz PASS data and increased the correlation (R^2) between hourly resolution denuded and ambient PASS b_{abs} from 0.59 to 0.70 and from 0.78 to 0.79 for 405 and 781 nm, respectively. All E_{abs} results based solely on PASS data have been calculated with vehicle plumes removed. Air was not scrubbed to remove NO_2 and O_3, and thus, it is possible that variations in the mixing ratios of these species may lead to minor drift in the b_{abs} measurements at 405 nm. Increases (or decreases) in NO_2 and O_3 mixing ratios within each 10 min period, after zeroing the PASS, could introduce a bias in the measured b_{abs} 405 nm. Measured mixing ratios for NO_2, derived as NO_x-NO (42i, Thermo Scientific, Waltham, MA) and O_3 (49i, Thermo Scientific, Waltham, MA), were reasonably stable at the site within each 10 min period, however, with mean relative standard deviations of 2.2% and 9.0%, respectively. No relationship was observed between mixing ratios for these species and calculated E_{abs} values. Relative humidity was not controlled for sampled air, and the ambient mean value was 59 ± 16% (1σ). To explore any potential impact of relative humidity on the PASS optical measurements, regressions were performed against b_{abs}, b_{sca}, MAC, and E_{abs} at both wavelengths. R^2 values were in the range of 0.00–0.05 in all cases. Temperature, relative humidity, NO_2, and O_3 mixing ratios as a function of time are provided in Figure S1 in the supporting information.

Mass absorption cross section (MAC) values were calculated by taking the ratio of the PASS-3 absorption data and the SP-AMS rBC mass concentration data for those periods when both instruments sampled ambient aerosol simultaneously (in this case vehicle events were not removed because both instruments sampled the same ensemble). For the last 4 days of the campaign (21–25 June 2014), the SP-AMS inlet was attached downstream of the automated valve, and thus, both the PASS-3 and SP-AMS instruments concurrently alternated between sampling ambient and thermally denuded aerosols every 10 min, enabling the calculation of MAC values for both ambient and denuded BC particles. The flow through the denuder was maintained at 6 L min^{-1} at all times using a bypass flow. The SP-AMS was operated at a flow rate of 0.085 L min^{-1}. Taking the ratio of each ambient MAC value and the mean-denuded MAC value represents a second means by which to assess absorption enhancement (E_{abs}) at hourly resolution for each wavelength, as shown in equation (2):

$$E_{abs} = \frac{\mathrm{MAC}_{\mathrm{ambient}}}{\mathrm{MAC}_{\mathrm{denuded\ (mean)}}} \tag{2}$$

The absorption Ångström exponent (α), which describes the wavelength dependence of aerosol absorption, was also calculated at hourly resolution from the b_{abs} values at 405 and 781 nm for ambient aerosol, as shown in equation (3):

$$\alpha = -\frac{\log\left(\frac{b_{abs,\ 405}}{b_{abs,\ 781}}\right)}{\log\left(\frac{405}{781}\right)} \tag{3}$$

Support measurements of particulate matter smaller than 2.5 μm in diameter ($PM_{2.5}$) mass concentration were taken using a Synchronized Hybrid Ambient Real-Time Particulate Monitor (SHARP model 5030, Thermo Fisher Scientific), which sampled air at 16.7 L min^{-1} at roof level (25 m above ground level) of the same building as the other instrumentation. The SHARP uses a combination of nephelometry (880 nm) and beta attenuation to measure $PM_{2.5}$ mass concentrations at 30 min resolution.

Modeled optical lensing absorption enhancement values based on Mie theory [*Bohren and Huffman*, 1983] were calculated using mean composition data for 100 and 400 nm (d_{va}) BC-containing particles from the SP-AMS (pToF mode) for the three periods discussed in section 3.4. These diameters were chosen based on the peaks of the bimodal mass-size distributions observed. Here we assume a core-shell spherical structure, a BC refractive index of 1.80 + 0.71i; a NR-PM_{BC} refractive index of 1.45 [*Moffet and Prather*, 2009; *Kim and Paulson*, 2013]; and densities of 1.8, 1.2, and 1.7 for BC, organics, and inorganics for the conversion of mass fractions to volume fractions and d_{va} to d_{ve} (volume equivalent diameter) [*Cappa et al.*, 2012]. It is assumed here that NR-PM is nonabsorbing. Modeled E_{abs} values were calculated at 405 nm and 781 nm using Python code [*Leinonen*, 2013] based on relationships described in *Bohren and Huffman* [1983]. Thermal denuding was found to remove, on average, 74% of NR-PM_{BC} by mass. Thus, lensing absorption enhancements for ambient BC relative to BC with 74% of NR-PM_{BC} removed were also calculated for comparison.

Air mass retroplumes were calculated using FLEXible PARTicle dispersion model "FLEXPART" in backward running mode, described in detail elsewhere [*Stohl et al.*, 2005], using European Centre for Medium-Range Weather Forecasts operational meteorological data at 1° × 1° resolution. The 20 day retroplumes consist of an emission sensitivity which, when combined with emission fluxes from a suitable inventory, can be used to determine source contributions. To quantify the contribution of emissions from boreal wildfires, Moderate Resolution Imaging Spectroradiometer (MODIS)-satellite hot spot data [*Giglio et al.*, 2003] and a simple emission scheme were used [*Stohl et al.*, 2007], with relevant emission factors for BC [*Andreae and Merlet*, 2001]. The FLEXPART calculations were carried out both for a passive tracer as well as a BC-like aerosol tracer, which was subject to dry and wet deposition [*Stohl et al.*, 2013]. It is important to note that the FLEXPART results cannot be used to quantify the contribution of local emissions within the Toronto urban area because of insufficient spatial resolution for both the available meteorological input data and emission inventories. However, the results are suitable for determining regional source contributions.

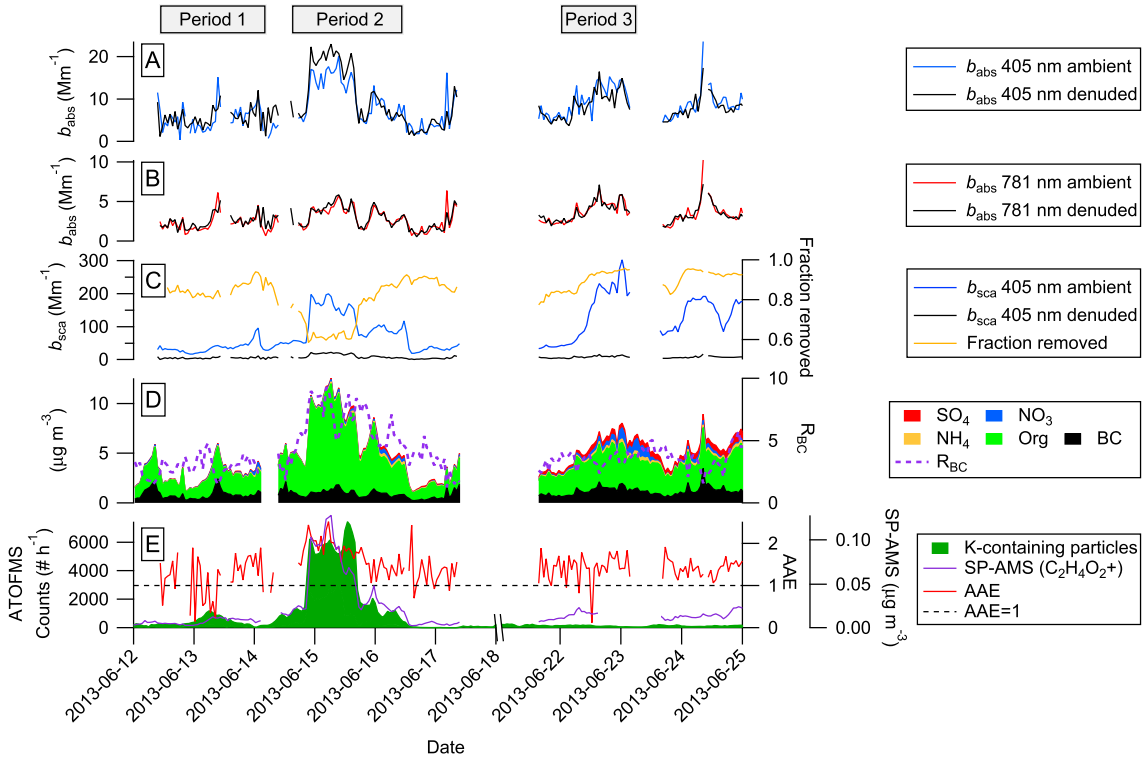

Figure 1. PASS absorption data for ambient and denuded aerosol at (a) 405 nm and (b) 781 nm. (c) PASS scattering coefficients for ambient and denuded aerosol (405 nm) and the fraction of scattering aerosol removed through thermal denuding. (d) SP-AMS mass concentrations of ambient BC, organics, ammonium, nitrate, and sulfate for BC-containing particles and the NR-PM_{BC}/BC ratio (R_{BC}). (e) The number of potassium-containing particles detected by the ATOFMS, the signal for ($C_2H_4O_2^+$) detected by the SP-AMS, and the aerosol absorption Ångström exponent (AAE). An AAE value of 1, often used to represent fossil fuel BC, is included for reference. The periods described in section 3.4 are also included at the top of the figure.

3. Results and Discussion

3.1. Impact of Thermal Denuding on Aerosol Absorption, Scattering, and Composition

The PASS absorption data for ambient particles and thermally denuded ambient particles detected from 12 to 25 June 2013 are shown in Figure 1. The thermally denuded aerosol absorption data have been corrected for transmission efficiency. Good temporal agreement is observed for absorption at 781 nm for ambient and denuded measurements performed within the same hour ($R^2 = 0.79$), as shown in Figure 2. Agreement is slightly poorer for the 405 nm absorption data ($R^2 = 0.70$), suggesting that thermal denuding may be affecting the absorption cross section of ambient aerosol to a greater extent at shorter wavelengths. The PASS scattering data for ambient and thermally denuded aerosols are also shown in Figure 1. Scattering at 405 nm is reasonably well correlated with $PM_{2.5}$ mass concentration at the site measured using the SHARP ($R^2 = 0.62$). A reduction of the PASS scattering signal after thermal denuding represents the removal of nonrefractory material both internally and/or externally mixed with ambient BC. The extent of internal/external mixing for NR-PM cannot be assessed using the SP-AMS configuration used here, however. The thermally denuded aerosol scattering data have also been corrected for transmission efficiency. The removal efficiency of scattering aerosol is above 80% for the majority of the sampling period, but drops to approximately 60% on 15 June, when the site was impacted by wildfire emissions, indicating the presence of low-volatility NR-PM during this event, as discussed below. Extremely low-volatility brown carbon (BrC) has been identified previously in biomass burning NR-PM_{BC} [*Saleh et al.*, 2014]. Effective removal of NR-PM_{BC} coatings is necessary, however, to investigate the magnitude of absorption enhancement that may be occurring through optical lensing [*Cappa et al.*, 2012]. The chemical composition of ambient BC-containing particles is also shown in Figure 1. The NR-PM_{BC}/BC ratio changes as a function of time, and the relative contributions of organics, ammonium, nitrate, and sulfate in NR-PM_{BC} also vary. Different NR-PM_{BC}/BC ratios (R_{BC}) and NR-PM_{BC} composition are observed when the

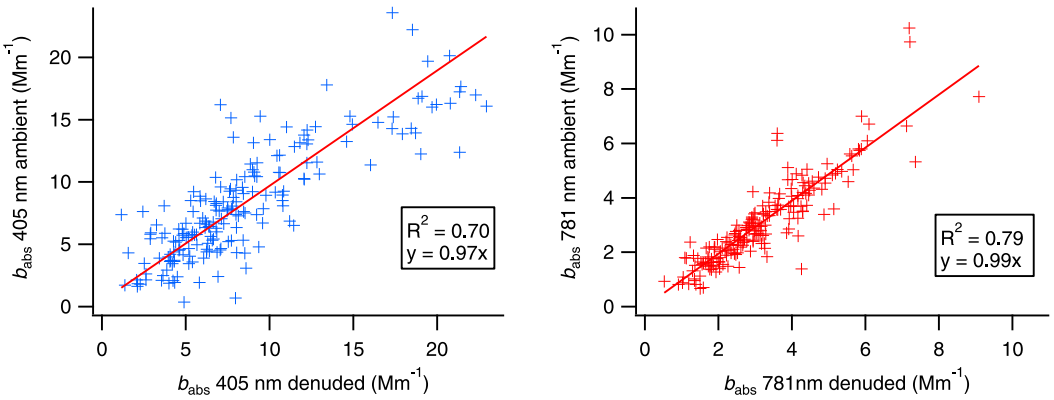

Figure 2. Linear regressions for PASS absorption data (405 and 781 nm) for ambient and denuded aerosol.

site is impacted by long-range transport events, discussed in detail in section 3.4. NR-PM_{BC} composition for thermally denuded BC was also measured for the last 4 days of the measurement campaign and is included in Figure S2. On average, 74% of the NR-PM_{BC} was evaporated in the denuder during this period.

3.2. Absorption Enhancement Based on PASS Data Exclusively

Absorption enhancement (E_{abs}) at 405 nm and 781 nm, calculated by taking the ratio of the PASS absorption data for ambient and denuded aerosols for each hour, is shown in Figure 3. A line representing the absence of any enhancement ($E_{abs} = 1$) has also been included for reference. No detectable increase in absorption due to lensing is observed using this approach during the campaign, and differences between the ambient and denuded b_{abs} data sets are not statistically significant at either wavelength ($P = 0.87$ and 0.66 for 405 nm and 781 nm, respectively). However, ambient b_{abs} values *lower* than denuded b_{abs} values were observed at 405 nm on 15 June (Figure 1). The observation of this effect, which is statistically significant during this period ($P < 0.05$), exclusively at 405 nm suggests that chemical transformation of organic aerosol during thermal denuding is likely occurring. In addition to the apparent negative absorption enhancement observed on 15 June, it can be seen from the b_{sca} data that the scattering aerosol, a fraction of which is

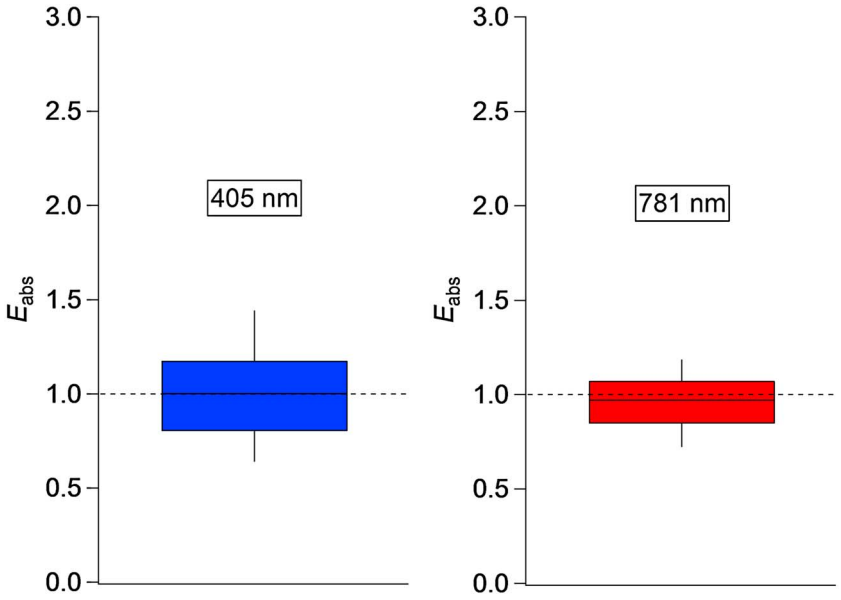

Figure 3. Absorption enhancement (E_{abs}) at 405 and 781 nm calculated as the ratio of ambient and denuded absorption data for each hour of the campaign ($N = 190$). The boxes and whiskers represent the 75th and 90th percentiles, respectively, and the solid horizontal lines represent the median. The dashed line represents no enhancement.

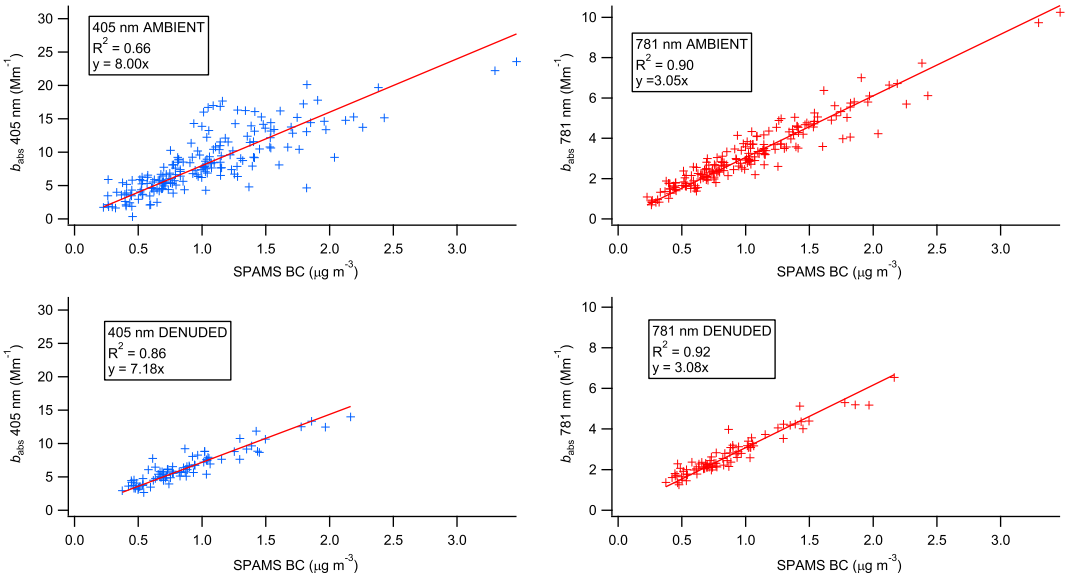

Figure 4. Relationship between PASS absorption at 405 nm and 781 nm and BC mass concentrations measured by the SP-AMS for (top) ambient and (bottom) denuded conditions. The mean MAC values at 405 nm are 8.42 and 7.49 $m^2\,g^{-1}$ for ambient and denuded BC, respectively. The mean MAC values at 781 nm are 3.19 and 3.21 $m^2\,g^{-1}$ for ambient and denuded BC, respectively.

internally mixed with BC, is not effectively evaporated in the denuder during this period (Figure 1). The observation of low-volatility biomass burning NR-PM_{BC} is in line with the work of *Saleh et al.* [2014] and is in contrast to the remainder of the campaign, where the removal efficiency of scattering aerosol is >80%. If BC coatings are not efficiently removed, calculations of absorption enhancement due to optical lensing will be underestimated using this approach. Thus, a second technique was also used to calculate E_{abs} at both wavelengths based on concurrent PASS and SP-AMS data [*Cappa et al.*, 2012; *McMeeking et al.*, 2014].

3.3. Absorption Enhancement Based on Simultaneous PASS and SP-AMS Data

The mass absorption cross section (MAC) of BC can be determined by relating the PASS absorption data with concurrent SP-AMS BC mass concentration data for those periods when both instruments measured ambient aerosol. This calculation is based on the assumption that BC is the only absorbing aerosol species. The temporal agreement between absorption and BC mass is shown in Figure 4 (top). There is a strong linear relationship between absorption at 781 nm and BC mass concentration at the site ($R^2 = 0.90$), with a mean MAC value for the entire campaign of 3.19 $m^2\,g^{-1}$. The relationship between absorption at 405 nm and BC mass concentration is weaker ($R^2 = 0.66$), suggesting that there may be additional absorption due to BrC at times during the measurement period. The mean MAC value determined for BC at 405 nm is 8.42 $m^2\,g^{-1}$. If absorption enhancement due to lensing is occurring, then the MAC value is expected to vary as a function of R_{BC} [*Lack and Cappa*, 2010; *Cappa et al.*, 2012; *McMeeking et al.*, 2014].

To derive an absorption enhancement value, it is necessary to first assess the MAC value for denuded BC at the site. For the last 4 days of the campaign the SP-AMS alternately sampled ambient and thermally denuded aerosols concurrently with the PASS. The mean MAC values derived for denuded BC were 3.21 and 7.49 $m^2\,g^{-1}$ for 781 nm and 405 nm, respectively (Figure 4, bottom). Assuming that these MAC values are representative of uncoated BC, if any enhancement due to lensing occurs, the MAC values observed for coated ambient BC should be higher. In fact, only 74% of the NR-PM was removed on average, as discussed below. While the difference between MAC values for ambient and denuded BC is negligible at 781 nm ($P = 0.78$), the difference at 405 nm is significant ($P < 0.01$). The mean MAC value observed for ambient BC at 405 nm (8.42 $m^2\,g^{-1}$) is 12% higher than the mean MAC value for denuded BC. Disentangling optical lensing absorption enhancement for BC and direct absorption by BrC can be difficult if the former effect is wavelength dependent [*Lack and Cappa*, 2010; *Lack and Langridge*, 2013]. However, absorption enhancement at 781 nm is nonetheless expected if optical lensing is occurring. The observation of

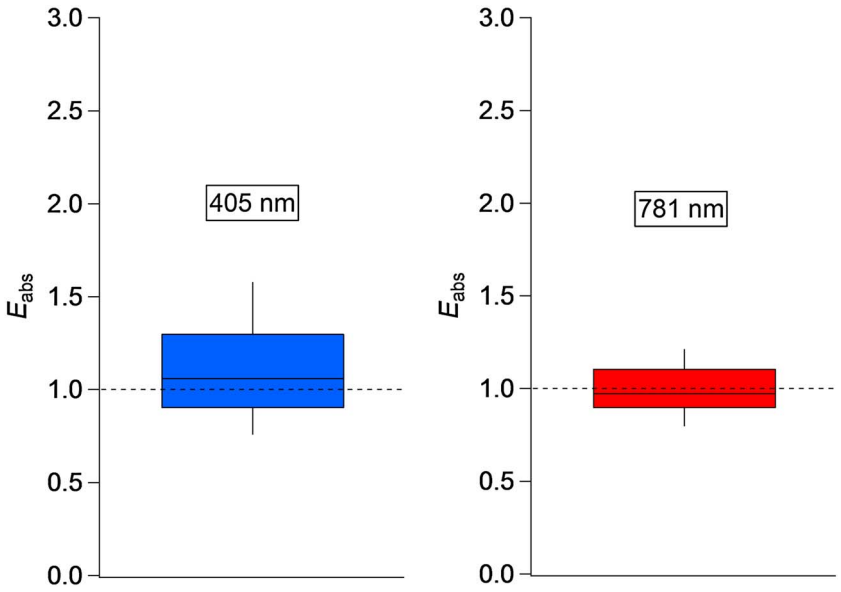

Figure 5. Absorption enhancement calculated as the ratio of MAC values (based on simultaneous PASS and SP-AMS data) to the single-mean MAC value determined for denuded rBC at 405 and 781 nm ($N = 184$). The boxes and whiskers represent the 75th and 90th percentiles, respectively, and the solid horizontal lines represent the median. The dashed line represents no enhancement.

absorption enhancement at 405 nm, and the absence of any enhancement at 781 nm, in this work suggests that direct absorption by BrC is relevant at this site [*Cappa et al.*, 2012; *Lack et al.*, 2012].

Hourly resolution absorption Ångström exponent (AAE) values, calculated from the b_{abs} values at 405 and 781 nm for ambient aerosol, are shown as a function of time in Figure 1. R_{BC} is also included for comparison. The highest AAE values are observed when R_{BC} is also highest, indicating that BC particles with large coatings and BrC, both internally and externally mixed, are detected simultaneously on 15 June. AAE values of 2 or higher are typically associated with BrC formed from the combustion of biomass [*Sandradewi et al.*, 2008; *Favez et al.*, 2010; *Healy et al.*, 2012; *McMeeking et al.*, 2014]. The number of potassium-containing particles, identified based on mass spectra for which *m/z* 39 is the most intense positive ion peak, also typically assigned to biomass burning sources [*Silva et al.*, 1999; *Healy et al.*, 2013; *Pagels et al.*, 2013], detected by the ATOFMS increase significantly during the same period, as does the SP-AMS signal for ($C_2H_4O_2^+$), a tracer for biomass combustion organic aerosol [*Alfarra et al.*, 2007] (Figure 1). The relationship between AAE and R_{BC} observed here is also consistent with laboratory measurements of biomass burning aerosol performed by *McMeeking et al.* [2014]. These findings indicate that the measurement site was impacted by biomass burning emissions during this period, as discussed in the next section.

By taking the ratio of each hourly ambient BC MAC value and the mean MAC value determined for denuded BC during the last 4 days of the campaign, E_{abs} values were calculated at hourly resolution as shown in Figure 5. This approach involves an inherent assumption that the absorption cross section of BC cores is independent of source and that the SP-AMS CE does not vary as a function of time. The MAC-based approach was determined to be more useful for the investigation of absorption enhancement than the PASS-only data approach in the case of this work, due to the ineffective removal of coating material in the thermal denuder and the potential modification of organic aerosol composition on 15 June (Figure S3). Mean E_{abs} values of 1.19 and 1.00 are observed at 405 and 781 nm, respectively, using the MAC-based approach. In order to investigate the influence of coating material on MAC-based E_{abs} further, three periods were selected, characterized by different air mass origin and R_{BC} values.

3.4. MAC Values and Absorption Enhancement for BC From Different Sources

FLEXPART retroplumes were used to identify three periods during which the site was impacted by BC of different origin as shown in Figure 6. During Period 1 (12 June 2013, 10:00 to 14 June 2013, 02:00), local

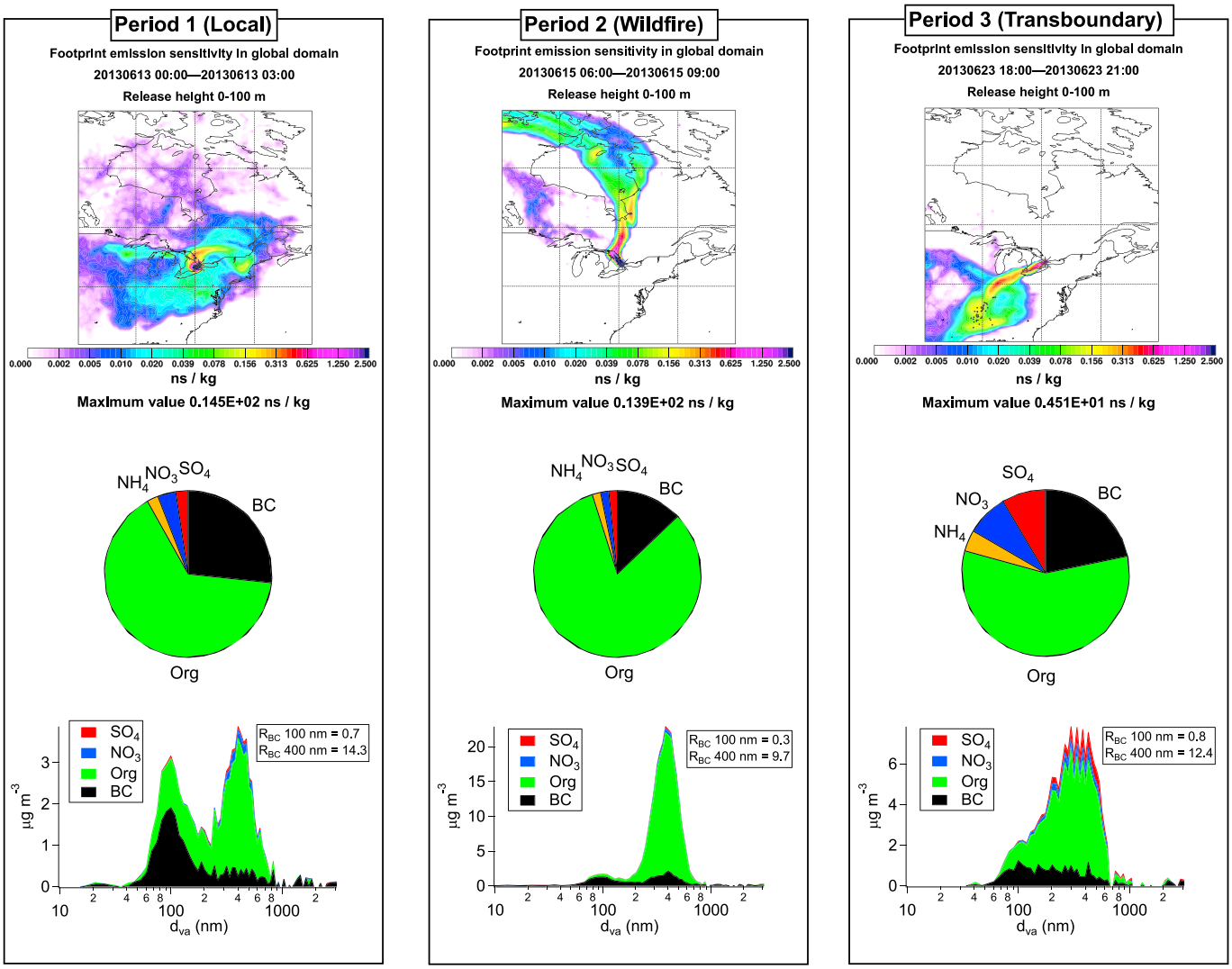

Figure 6. (top) FLEXPART retroplumes, (middle) SP-AMS BC particle bulk composition, and (bottom) SP-AMS size-resolved BC particle bulk composition, for the three periods defined in section 3.4. The black spots in the retroplume figures correspond to active wildfires identified using MODIS hot spot data.

emissions of BC are predicted to dominate at the sampling site, with minimal influence from BC originating outside southern Ontario. During Period 2 (14 June 2013, 14:00 to 16 June 2013, 11:00), wildfires in Quebec, identified using MODIS data, are predicted to influence the site. Finally, during Period 3 (22 June 2013, 00:00 to 23 June 2013, 03:00), transboundary emissions, associated predominantly with fossil fuel combustion in the United States [*Jeong et al.*, 2013], are predicted to impact the site. While small wildfires were also identified in the U.S. during Period 3 and are visible in the retroplume plot (Figure 6), these are predicted to contribute very little BC relative to the significant anthropogenic sources in the region. This is supported by the relatively low numbers of potassium-containing particles detected using the ATOFMS during Period 3 (Figure 1).

The chemical composition of NR-PM_{BC} and the mass-size distribution of BC particles differ for the three periods, as shown in Figure 6. During Period 1, the majority of BC mass is associated with particles smaller than 200 nm in diameter, characterized by a mode at 100 nm ($R_{BC} = 0.7$) and relatively thin organic coatings. A second mode is also apparent at 400 nm ($R_{BC} = 14.3$) featuring less BC mass but thicker coatings, dominated by organics. The mean bulk R_{BC} is 3.0. The smaller BC particles during this period are most likely associated predominantly with local vehicular emissions [*Lee et al.*, 2015]. High-resolution mass spectra of NR-PM_{BC} organics for this period also contain hydrocarbon contributions consistent with vehicle

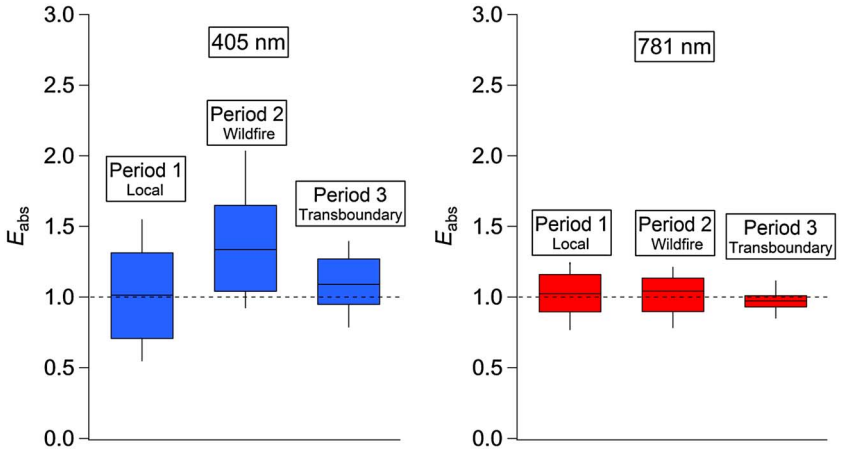

Figure 7. Absorption enhancement calculated as the ratio of MAC values (based on simultaneous PASS and SP-AMS data) to the single-mean MAC value determined for denuded rBC at 405 and 781 nm for the three periods described in section 3.4. The boxes and whiskers represent the 75th and 90th percentiles, respectively, and the solid horizontal lines represent the median. $N = 36$, 44, and 36 for Periods 1, 2, and 3, respectively. The dashed line represents no enhancement.

emissions (Figure S4) [*Massoli et al.*, 2012]. The larger mode may represent urban and/or regional background BC. During Period 2, BC mass is almost evenly distributed between two modes, one at 100 nm ($R_{BC} = 0.3$) and one at 400 nm ($R_{BC} = 9.7$), with a mean bulk R_{BC} of 6.9. While the smaller BC particles exhibit relatively thin coatings, and are expected to be associated with local emissions, the larger BC particles are characterized by much thicker coatings comprised almost entirely of organics. These larger particles are attributed to wildfire emissions in Quebec, and the increase in the aerosol AAE determined using PASS data, the number of potassium-rich particles detected by ATOFMS, and the SP-AMS signal for ($C_2H_4O_2^+$) on 15 June support this assignment (Figure 1). High-resolution mass spectra of NR-PM_{BC} organics for this period also contain tracer ions consistent with biomass burning emissions (Figure S4) [*Alfarra et al.*, 2007]. During Period 3, BC mass is spread across a broad size mode with a mean bulk R_{BC} of 3.7. Again, smaller BC particles (100 nm, $R_{BC} = 0.8$) are characterized by thin organic coatings, and are likely associated with local emissions, but larger BC particles (400 nm, $R_{BC} = 12.4$) feature thicker coatings, composed of organics, ammonium, sulphate, and nitrate. The higher mass fractions of sulfate and nitrate observed for the coatings in Period 3 suggest that these BC particles are either emitted through fossil fuel combustion or have mixed with fossil fuel combustion emissions during transport to Toronto. High-resolution mass spectra of NR-PM_{BC} organics for this period are characterized by much lower signals for tracer ions associated with vehicular emissions and biomass burning (Figure S4).

MAC-based E_{abs} values for each period are shown in Figure 7. No significant enhancement is observed at 781 nm for any of the three periods. However, high E_{abs} values at 405 nm are observed during Period 2 in particular (mean = 1.39). These findings indicate that absorption by BrC, and not optical lensing, is driving the aerosol absorption enhancement observed in Toronto. By comparison, Mie theory calculations based on SP-AMS pToF mode composition data for each period predict significant optical lensing absorption enhancement at both wavelengths. The predicted optical lensing absorption enhancements at 781 nm, based on a mass-weighted average for 100 and 400 nm (d_{va}) BC-containing particles, are 1.23, 1.56, and 1.34 for Periods 1, 2, and 3, respectively. Thus, E_{abs} predictions based on composition and core-shell Mie theory would result in an overestimation of BC radiative forcing in the region. It is important to note that these calculations are based on absorption for coated BC relative to bare BC cores. However, only 74% of the NR-PM_{BC} by mass was removed in the denuder in this work. Thus, absorption enhancements for ambient BC particles relative to the same particles with 74% of NR-PM_{BC} removed were also calculated. These predicted E_{abs} values better represent the enhancements that would be measured using the approach described in this work. The predicted optical lensing absorption enhancements at 781 nm for BC-containing particles (relative to the same particles with 74% of their coating material removed), assuming concentric core-shell morphology, are 1.11, 1.21, and 1.14 for Periods 1, 2, and 3, respectively.

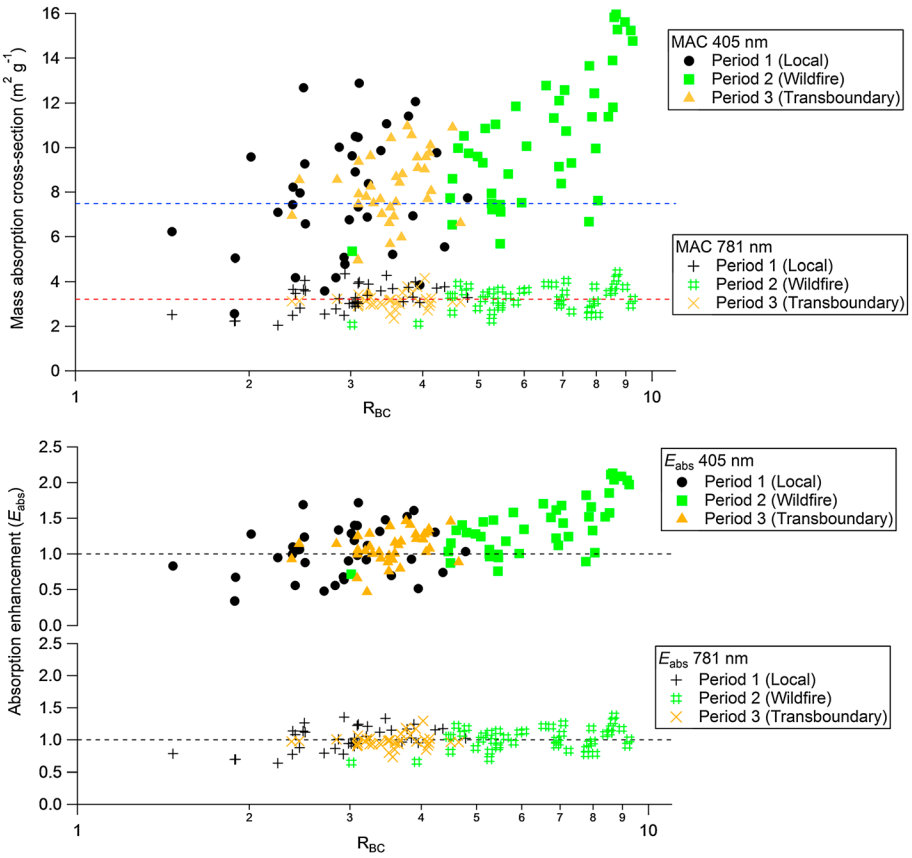

Figure 8. The 405 and 781 nm MAC values for (top) ambient aerosol and (bottom) E_{abs} values as a function of R_{BC} for the three periods described in section 3.4. The blue and red dashed lines represent the mean MAC values determined for denuded BC at 405 and 781 nm, respectively. The black dashed line represents $E_{abs} = 1$.

Thus, the measured E_{abs} values reported here are not consistent with the core-shell model prediction for coated BC particles.

As shown in Figure 8, a weak dependence of MAC value upon R_{BC} is apparent for the three periods, with the highest MAC values at 405 nm observed during Period 2. No dependence of MAC value upon R_{BC} is apparent at 781 nm. MAC-based E_{abs} values for the three periods are also included as a function of R_{BC} in Figure 8. E_{abs} values at 405 nm greater than 2 are observed during Period 2, when the site was impacted by BC associated with wildfires in Quebec. The relationship between MAC value and R_{BC} observed during Period 2 is consistent with recent laboratory measurements of biomass burning aerosol performed by *McMeeking et al.* [2014]. In that case, MAC-based absorption enhancements at 405 nm for aerosol generated in a series of controlled wood burns were also ~2 in the R_{BC} range of 7–10.

The absence of any absorption enhancement attributable to lensing at 781 nm for ambient BC in this work is consistent with E_{abs} values determined by *Cappa et al.* [2012] for urban fossil fuel BC of varying photochemical age in California. In that case, minimal absorption enhancement was also observed for $R_{BC} < 10$. The observation of an absorption enhancement at 405 nm in this work, attributable to the presence of BrC, is also consistent with photoacoustic absorption measurements of an ambient biomass burning plume performed by *Lack et al.* [2012]. Lack et al. also observed an absorption enhancement at 532 nm that was not dependent upon primary particulate organic matter mass concentration. This suggested that the enhancement at 532 nm was attributable to lensing in that case. However, there is no evidence for any lensing effect in this work. The absence of any absorption enhancement attributable to lensing is in contrast with previous ambient measurements of BC absorption performed previously in Toronto, however. *Knox et al.* [2009] calculated E_{abs} for BC using photoacoustic absorption data (760 nm) and elemental carbon mass concentrations determined using thermal/optical analysis. Ambient MAC

values (760 nm) did not vary significantly as a function of time, in agreement with the 781 nm data in this work. However, thermally denuded BC (340°C) MAC values (760 nm) were found to be lower than corresponding ambient BC MAC values. Specifically, mean E_{abs} values (760 nm) of 1.2, 1.4, and ~1 were determined for periods dominated by "fresh," semiaged, and "aged" aerosols in that case. This observation was attributed to efficient removal of coating material for fresh and semiaged aerosols and inefficient removal of coating material in the case of aged aerosol. However, in the absence of online measurements of thermally denuded NR-PM_{BC} composition in that case, this effect could not be confirmed directly. Different instrumentation was used to quantify BC mass, and the measurements performed by *Knox et al*. [2009] took place during the winter, while the measurements performed in this work took place in the summer. Thus, it is possible that BC mixing state is not directly comparable for these two campaigns. The absence of any optical lensing absorption enhancement for BC in this work is consistent with previous measurements using a particle soot absorption photometer in rural Ontario in the summer, however [*Chan et al*., 2010].

4. Conclusions

Two approaches were explored for the assessment of absorption enhancement for BC at an urban site in Toronto, Canada. During the measurement period, the site was influenced by regional emissions, wildfire emissions originating in Quebec, and transboundary fossil fuel emissions originating in the U.S. Thermal denuding was found to be ineffective for the complete removal of organic aerosol coatings on wildfire BC particles and also altered the absorption efficiency of the organic aerosol itself. This led to apparent negative absorption enhancements at 405 nm when PASS data were used exclusively to calculate E_{abs} and represents a shortcoming of this approach. Thus, a MAC-based approach was determined to be more useful for the investigation of absorption enhancement in this case. No detectable E_{abs} was observed for BC at 781 nm using either method, irrespective of BC source or R_{BC}, indicating that optical lensing is not relevant for Toronto, at least in the summer months. It is important to note that the E_{abs} values reported here represent a minimum, due to the incomplete removal of the coating material (74%). However, removal of this fraction should nonetheless result in detectable E_{abs} according to Mie theory calculations based on the measured BC particle diameters and composition. An enhancement in absorption at 405 nm, attributed to direct absorption by brown carbon associated with wildfire emissions in Quebec, was observed however. Brown carbon absorption accounted for more than 50% of direct absorption at 405 nm at times during this event. These findings indicate that wildfire emissions originating outside Ontario can affect regional warming in the province through direct absorption by both BC and brown carbon. The absence of any optical lensing effect for internally mixed wildfire BC, or transboundary fossil fuel BC, detected in this work supports the argument that inclusion of lensing-related absorption enhancement in climate models may lead to an overestimation of positive radiative forcing impacts. These findings may also be applicable to other urban or remote locations influenced by aged, transported BC.

Acknowledgments
This work has been funded by the Marie Curie Action FP7-PEOPLE-IOF-2011 (project CHEMBC, 299755). All data used for the preparation of this manuscript are freely available on request through the corresponding author (robert.healy@utoronto.ca).

References

Adachi, K., and P. R. Buseck (2013), Changes of ns-soot mixing states and shapes in an urban area during CalNex, *J. Geophys. Res. Atmos.*, *118*, 3723–3730, doi:10.1002/jgrd.50321.

Adachi, K., S. H. Chung, and P. R. Buseck (2010), Shapes of soot aerosol particles and implications for their effects on climate, *J. Geophys. Res.*, *115*, D15206, doi:10.1029/2009JD012868.

Alfarra, M. R., A. S. H. Prevot, S. Szidat, J. Sandradewi, S. Weimer, V. A. Lanz, D. Schreiber, M. Mohr, and U. Baltensperger (2007), Identification of the mass spectral signature of organic aerosols from wood burning emissions, *Environ. Sci. Technol.*, *41*(16), 5770–5777, doi:10.1021/es062289b.

Andreae, M. O., and P. Merlet (2001), Emission of trace gases and aerosols from biomass burning, *Global Biogeochem. Cycles*, *15*(4), 955–966, doi:10.1029/2000GB001382.

Arnott, P. W., H. Moosmüller, C. Fred Rogers, T. Jin, and R. Bruch (1999), Photoacoustic spectrometer for measuring light absorption by aerosol: Instrument description, *Atmos. Environ.*, *33*(17), 2845–2852, doi:10.1016/s1352-2310(98)00361-6.

Bohren, C. F., and D. R. Huffman (1983), *Absorption and Scattering of Light by Small Particles*, John Wiley, New York.

Bond, T. C., G. Habib, and R. W. Bergstrom (2006), Limitations in the enhancement of visible light absorption due to mixing state, *J. Geophys. Res.*, *111*, D20211, doi:10.1029/2006JD007315.

Bond, T. C., et al. (2013), Bounding the role of black carbon in the climate system: A scientific assessment, *J. Geophys. Res. Atmos.*, *118*, 5380–5552, doi:10.1002/jgrd.50171.

Cappa, C. D., et al. (2012), Radiative absorption enhancements due to the mixing state of atmospheric black carbon, *Science*, *337*(6098), 1078–1081, doi:10.1126/science.1223447.

Chan, T. W., et al. (2010), Observations of OM/OC and specific attenuation coefficients (SAC) in ambient fine PM at a rural site in central Ontario, Canada, *Atmos. Chem. Phys.*, *10*(5), 2393–2411, doi:10.5194/acp-10-2393-2010.

Chan, T. W., J. R. Brook, G. J. Smallwood, and G. Lu (2011), Time-resolved measurements of black carbon light absorption enhancement in urban and near-urban locations of southern Ontario, Canada, *Atmos. Chem. Phys.*, *11*(20), 10,407–10,432, doi:10.5194/acp-11-10407-2011.

China, S., C. Mazzoleni, K. Gorkowski, A. C. Aiken, and M. K. Dubey (2013), Morphology and mixing state of individual freshly emitted wildfire carbonaceous particles, *Nat. Commun.*, *4*, doi:10.1038/ncomms3122.

Corbin, J. C., B. Sierau, M. Gysel, M. Laborde, A. Keller, J. Kim, A. Petzold, T. B. Onasch, U. Lohmann, and A. A. Mensah (2014), Mass spectrometry of refractory black carbon particles from six sources: Carbon-cluster and oxygenated ions, *Atmos. Chem. Phys.*, *14*(5), 2591–2603, doi:10.5194/acp-14-2591-2014.

Cross, E. S., T. B. Onasch, M. Canagaratna, J. T. Jayne, J. Kimmel, X. Y. Yu, M. L. Alexander, D. R. Worsnop, and P. Davidovits (2009), Single particle characterization using a light scattering module coupled to a time-of-flight aerosol mass spectrometer, *Atmos. Chem. Phys.*, *9*(20), 7769–7793, doi:10.5194/acp-9-7769-2009.

Favez, O., et al. (2010), Inter-comparison of source apportionment models for the estimation of wood burning aerosols during wintertime in an Alpine City (Grenoble, France), *Atmos. Chem. Phys.*, *10*(12), 5295–5314, doi:10.5194/acp-10-5295-2010.

Flowers, B. A., M. K. Dubey, C. Mazzoleni, E. A. Stone, J. J. Schauer, S. W. Kim, and S. C. Yoon (2010), Optical-chemical-microphysical relationships and closure studies for mixed carbonaceous aerosols observed at Jeju Island; 3-laser photoacoustic spectrometer, particle sizing, and filter analysis, *Atmos. Chem. Phys.*, *10*(21), 10,387–10,398, doi:10.5194/acp-10-10387-2010.

Fuller, K. A., W. C. Malm, and S. M. Kreidenweis (1999), Effects of mixing on extinction by carbonaceous particles, *J. Geophys. Res.*, *104*(D13), 15,941–15,954, doi:10.1029/1998JD100069.

Gard, E., J. E. Mayer, B. D. Morrical, T. Dienes, D. P. Fergenson, and K. A. Prather (1997), Real-time analysis of individual atmospheric aerosol particles: Design and performance of a portable ATOFMS, *Anal. Chem.*, *69*(20), 4083–4091, doi:10.1021/ac970540n.

Giglio, L., J. Descloitres, C. O. Justice, and Y. J. Kaufman (2003), An enhanced contextual fire detection algorithm for MODIS, *Remote Sens. Environ.*, *87*(2–3), 273–282, doi:10.1016/S0034-4257(03)00184-6.

Gross, D. S., et al. (2010), Environmental chemistry through intelligent atmospheric data analysis, *Environ. Modell. Software*, *25*, 760–769, doi:10.1016/j.envsoft.2009.12.001.

Guo, X., T. Nakayama, H. Yamada, S. Inomata, K. Tonokura, and Y. Matsumi (2014), Measurement of the light absorbing properties of diesel exhaust particles using a three-wavelength photoacoustic spectrometer, *Atmos. Environ.*, *94*(0), 428–437, doi:10.1016/j.atmosenv.2014.05.042.

Healy, R. M., et al. (2012), Sources and mixing state of size-resolved elemental carbon particles in a European megacity: Paris, *Atmos. Chem. Phys.*, *12*(4), 1681–1700, doi:10.5194/acp-12-1681-2012.

Healy, R. M., et al. (2013), Quantitative determination of carbonaceous particle mixing state in Paris using single-particle mass spectrometer and aerosol mass spectrometer measurements, *Atmos. Chem. Phys.*, *13*(18), 9479–9496, doi:10.5194/acp-13-9479-2013.

Horvath, H. (1993), Atmospheric light absorption—A review, *Atmos. Environ. Part A*, *27*(3), 293–317, doi:10.1016/0960-1686(93)90104-7.

Intergovernmental Panel on Climate Change (2013), *Climate Change 2013: The Physical Science Basis. Contribution of Working Group I to the Fifth Assessment Report of the Intergovernmental Panel on Climate Change*, Cambridge Univ. Press, Cambridge, U. K., and New York, doi:10.1017/CBO9781107415324.004.

Jacobson, M. Z. (2000), A physically based treatment of elemental carbon optics: Implications for global direct forcing of aerosols, *Geophys. Res. Lett.*, *27*(2), 217–220, doi:10.1029/1999GL010968.

Jacobson, M. Z. (2001), Strong radiative heating due to the mixing state of black carbon in atmospheric aerosols, *Nature*, *409*(6821), 695–697.

Jeong, C. H., M. L. McGuire, D. Herod, T. Dann, E. Dabek-Zlotorzynska, D. Wang, L. Ding, V. Celo, D. Mathieu, and G. J. Evans (2011), Receptor model based identification of $PM_{2.5}$ sources in Canadian cities, *Atmos. Pollut. Res.*, *2*(2), 158–171.

Jeong, C.-H., D. Herod, E. Dabek-Zlotorzynska, L. Ding, M. L. McGuire, and G. Evans (2013), Identification of the sources and geographic origins of black carbon using factor analysis at paired rural and urban sites, *Environ. Sci. Technol.*, *47*(15), 8462–8470, doi:10.1021/es304695t.

Jimenez, J. L., et al. (2003), Ambient aerosol sampling using the Aerodyne Aerosol Mass Spectrometer, *J. Geophys. Res.*, *108*(D7), 8425, doi:10.1029/2001JD001213.

Khalizov, A. F., H. Xue, L. Wang, J. Zheng, and R. Zhang (2009), Enhanced light absorption and scattering by carbon soot aerosol internally mixed with sulfuric acid, *J. Phys. Chem. A*, *113*(6), 1066–1074, doi:10.1021/jp807531n.

Kim, H., and S. E. Paulson (2013), Real refractive indices and volatility of secondary organic aerosol generated from photooxidation and ozonolysis of limonene, α-pinene and toluene, *Atmos. Chem. Phys.*, *13*(15), 7711–7723, doi:10.5194/acp-13-7711-2013.

Knox, A., G. J. Evans, J. R. Brook, X. Yao, C.-H. Jeong, K. J. Godri, K. Sabaliauskas, and J. G. Slowik (2009), Mass absorption cross-section of ambient black carbon aerosol in relation to chemical age, *Aerosol Sci. Technol.*, *43*(6), 522–532.

Lack, D. A., and C. D. Cappa (2010), Impact of brown and clear carbon on light absorption enhancement, single scatter albedo and absorption wavelength dependence of black carbon, *Atmos. Chem. Phys.*, *10*(9), 4207–4220, doi:10.5194/acp-10-4207-2010.

Lack, D. A., and J. M. Langridge (2013), On the attribution of black and brown carbon light absorption using the Ångström exponent, *Atmos. Chem. Phys.*, *13*(20), 10,535–10,543, doi:10.5194/acp-13-10535-2013.

Lack, D. A., C. D. Cappa, E. S. Cross, P. Massoli, A. T. Ahern, P. Davidovits, and T. B. Onasch (2009), Absorption enhancement of coated absorbing aerosols: Validation of the photo-acoustic technique for measuring the enhancement, *Aerosol Sci. Technol.*, *43*(10), 1006–1012, doi:10.1080/02786820903117932.

Lack, D. A., J. M. Langridge, R. Bahreini, C. D. Cappa, A. M. Middlebrook, and J. P. Schwarz (2012), Brown carbon and internal mixing in biomass burning particles, *Proc. Natl. Acad. Sci. U.S.A.*, *109*(37), 14,802–14,807, doi:10.1073/pnas.1206575109.

Lan, Z.-J., X.-F. Huang, K.-Y. Yu, T.-L. Sun, L.-W. Zeng, and M. Hu (2013), Light absorption of black carbon aerosol and its enhancement by mixing state in an urban atmosphere in south China, *Atmos. Environ.*, *69*(0), 118–123, doi:10.1016/j.atmosenv.2012.12.009.

Lee, A. K. Y., M. D. Willis, R. M. Healy, T. B. Onasch, and J. P. D. Abbatt (2015), Mixing state of carbonaceous aerosol in an urban environment: Single particle characterization using the soot particle aerosol mass spectrometer (SP-AMS), *Atmos. Chem. Phys.*, *15*(4), 1823–1841, doi:10.5194/acp-15-1823-2015.

Leinonen, J. (2013), Python code for calculating Mie scattering from single- and dual-layered spheres. [Available at http://code.google.com/p/pymiecoated/.]

Liu, D., J. Allan, J. Whitehead, D. Young, M. Flynn, H. Coe, G. McFiggans, Z. L. Fleming, and B. Bandy (2013), Ambient black carbon particle hygroscopic properties controlled by mixing state and composition, *Atmos. Chem. Phys.*, *13*(4), 2015–2029, doi:10.5194/acp-13-2015-2013.

Liu, D., J. W. Taylor, D. E. Young, M. J. Flynn, H. Coe, and J. D. Allan (2015), The effect of complex black carbon microphysics on the determination of the optical properties of brown carbon, *Geophys. Res. Lett.*, *42*, 613–619, doi:10.1002/2014GL062443.

Liu, L., M. I. Mishchenko, and P. W. Arnott (2008), A study of radiative properties of fractal soot aggregates using the superposition T-matrix method, *J. Quant. Spectrosc. Radiat. Transfer*, *109*(15), 2656–2663, doi:10.1016/j.jqsrt.2008.05.001.

Martin, M., et al. (2013), Hygroscopic properties of fresh and aged wood burning particles, *J. Aerosol Sci.*, *56*(0), 15–29, doi:10.1016/j.jaerosci.2012.08.006.

Massoli, P., et al. (2012), Pollution gradients and chemical characterization of particulate matter from vehicular traffic near major roadways: Results from the 2009 Queens College Air Quality Study in NYC, *Aerosol Sci. Technol.*, *46*(11), 1201–1218, doi:10.1080/02786826.2012.701784.

McMeeking, G. R., E. Fortner, T. B. Onasch, J. W. Taylor, M. Flynn, H. Coe, and S. M. Kreidenweis (2014), Impacts of nonrefractory material on light absorption by aerosols emitted from biomass burning, *J. Geophys. Res. Atmos.*, *119*, 12,272–12,286, doi:10.1002/2014JD021750.

Moffet, R. C., and K. A. Prather (2009), In-situ measurements of the mixing state and optical properties of soot with implications for radiative forcing estimates, *Proc. Natl. Acad. Sci. U.S.A.*, *106*(29), 11,872–11,877, doi:10.1073/pnas.0900040106.

Mohr, C., et al. (2013), Contribution of nitrated phenols to wood burning brown carbon light absorption in Detling, United Kingdom during winter time, *Environ. Sci. Technol.*, *47*(12), 6316–6324, doi:10.1021/es400683v.

Moosmüller, H., R. K. Chakrabarty, and W. P. Arnott (2009), Aerosol light absorption and its measurement: A review, *J. Quant. Spectros. Radiat. Transfer*, *110*(11), 844–878, doi:10.1016/j.jqsrt.2009.02.035.

Nakayama, T., Y. Ikeda, Y. Sawada, Y. Setoguchi, S. Ogawa, K. Kawana, M. Mochida, F. Ikemori, K. Matsumoto, and Y. Matsumi (2014), Properties of light-absorbing aerosols in the Nagoya urban area, Japan, in August 2011 and January 2012: Contributions of brown carbon and lensing effect, *J. Geophys. Res. Atmos.*, *119*, 12,721–12,739, doi:10.1002/2014JD021744.

Onasch, T. B., A. Trimborn, E. C. Fortner, J. T. Jayne, G. L. Kok, L. R. Williams, P. Davidovits, and D. R. Worsnop (2012), Soot particle aerosol mass spectrometer: development, validation, and initial application, *Aerosol Sci. Technol.*, *46*(7), 804–817, doi:10.1080/02786826.2012.663948.

Pagels, J., D. D. Dutcher, M. R. Stolzenburg, P. H. McMurry, M. E. Gälli, and D. S. Gross (2013), Fine-particle emissions from solid biofuel combustion studied with single-particle mass spectrometry: Identification of markers for organics, soot, and ash components, *J. Geophys. Res. Atmos.*, *118*, 859–870, doi:10.1029/2012JD018389.

Rebotier, T. P., and K. A. Prather (2007), Aerosol time-of-flight mass spectrometry data analysis: A benchmark of clustering algorithms, *Anal. Chim. Acta*, *585*(1), 38–54, doi:10.1016/j.aca.2006.12.009.

Riemer, N., H. Vogel, and B. Vogel (2004), Soot aging time scales in polluted regions during day and night, *Atmos. Chem. Phys.*, *4*(7), 1885–1893, doi:10.5194/acp-4-1885-2004.

Sabaliauskas, K., C.-H. Jeong, X. Yao, and G. J. Evans (2014), The application of wavelet decomposition to quantify the local and regional sources of ultrafine particles in cities, *Atmos. Environ.*, *95*(0), 249–257, doi:10.1016/j.atmosenv.2014.05.035.

Saleh, R., et al. (2014), Brownness of organics in aerosols from biomass burning linked to their black carbon content, *Nat. Geosci.*, *7*(9), 647–650, doi:10.1038/ngeo2220.

Sandradewi, J., A. S. H. Prévôt, S. Szidat, N. Perron, M. R. Alfarra, V. A. Lanz, E. Weingartner, and U. Baltensperger (2008), Using aerosol light absorption measurements for the quantitative determination of wood burning and traffic emission contributions to particulate matter, *Environ. Sci. Technol.*, *42*(9), 3316–3323, doi:10.1021/es702253m.

Schnaiter, M., C. Linke, O. Möhler, K. H. Naumann, H. Saathoff, R. Wagner, U. Schurath, and B. Wehner (2005), Absorption amplification of black carbon internally mixed with secondary organic aerosol, *J. Geophys. Res.*, *110*, D19204, doi:10.1029/2005JD006046.

Schnitzler, E. G., A. Dutt, A. M. Charbonneau, J. S. Olfert, and W. Jäger (2014), Soot aggregate restructuring due to coatings of secondary organic aerosol derived from aromatic precursors, *Environ. Sci. Technol.*, *48*(24), 14,309–14,316, doi:10.1021/es503699b.

Schwarz, J. P., et al. (2008), Measurement of the mixing state, mass, and optical size of individual black carbon particles in urban and biomass burning emissions, *Geophys. Res. Lett.*, *35*, L13810, doi:10.1029/2008GL033968.

Sedlacek, A. J., E. R. Lewis, L. Kleinman, J. Xu, and Q. Zhang (2012), Determination of and evidence for non-core-shell structure of particles containing black carbon using the single-particle soot photometer (SP2), *Geophys. Res. Lett.*, *39*, L06802, doi:10.1029/2012GL050905.

Silva, P. J., D. Y. Liu, C. A. Noble, and K. A. Prather (1999), Size and chemical characterization of individual particles resulting from biomass burning of local Southern California species, *Environ. Sci. Technol.*, *33*(18), 3068–3076.

Stier, P., J. H. Seinfeld, S. Kinne, J. Feichter, and O. Boucher (2006), Impact of nonabsorbing anthropogenic aerosols on clear-sky atmospheric absorption, *J. Geophys. Res.*, *111*, D18201, doi:10.1029/2006JD007147.

Stohl, A., C. Forster, A. Frank, P. Seibert, and G. Wotawa (2005), Technical note: The Lagrangian particle dispersion model FLEXPART version 6.2, *Atmos. Chem. Phys.*, *5*(9), 2461–2474, doi:10.5194/acp-5-2461-2005.

Stohl, A., et al. (2007), Arctic smoke—Record high air pollution levels in the European Arctic due to agricultural fires in eastern Europe in spring 2006, *Atmos. Chem. Phys.*, *7*(2), 511–534, doi:10.5194/acp-7-511-2007.

Stohl, A., Z. Klimont, S. Eckhardt, K. Kupiainen, V. P. Shevchenko, V. M. Kopeikin, and A. N. Novigatsky (2013), Black carbon in the Arctic: The underestimated role of gas flaring and residential combustion emissions, *Atmos. Chem. Phys.*, *13*(17), 8833–8855, doi:10.5194/acp-13-8833-2013.

Su, Y., M. F. Sipin, H. Furutani, and K. A. Prather (2004), Development and characterization of an aerosol time-of-flight mass spectrometer with increased detection efficiency, *Anal. Chem.*, *76*(3), 712–719, doi:10.1021/ac034797z.

Wang, J. M., C. H. Jeong, N. Zimmerman, R. M. Healy, D. K. Wang, F. Ke, and G. J. Evans (2015), Plume-based analysis of vehicle fleet air pollutant emissions and the contribution from high emitters, *Atmos. Meas. Tech. Discuss.*, *8*(3), 2881–2912, doi:10.5194/amtd-8-2881-2015.

Weingartner, E., U. Baltensperger, and H. Burtscher (1995), Growth and structural change of combustion aerosols at high relative humidity, *Environ. Sci. Technol.*, *29*(12), 2982–2986, doi:10.1021/es00012a014.

Willis, M. D., A. K. Y. Lee, T. B. Onasch, E. C. Fortner, L. R. Williams, A. T. Lambe, D. R. Worsnop, and J. P. D. Abbatt (2014), Collection efficiency of the soot-particle aerosol mass spectrometer (SP-AMS) for internally mixed particulate black carbon, *Atmos. Meas. Tech.*, *7*(12), 4507–4516, doi:10.5194/amt-7-4507-2014.